Baggio, Mariangela; Tamminen, Aleksi; Ala-Laurinaho, Juha; Taylor, Zachary

Design of double-reflector objective for corneal sensing in the 220-330 GHz band

Published in:
2022 16th European Conference on Antennas and Propagation, EuCAP 2022

DOI:
10.23919/EuCAP53622.2022.9769685

Published: 01/01/2022

Document Version
Peer-reviewed accepted author manuscript, also known as Final accepted manuscript or Post-print

Design of double-reflector objective for corneal sensing in the 220 – 330 GHz band

Mariangela Baggio, Aleksi Tamminen, Juha Ala-Laurinaho, Zachary Taylor
Department of Electronics and Nanoengineering, Aalto University, Espoo, Finland, mariangela.baggio@aalto.fi

***Abstract*- An all reflective, Schwarzschild objective design for corneal reflectometry is evaluated in the WR3.4 (220-330 GHz) frequency band. The shadow created by the 60-mm diameter secondary mirror is sufficiently large to mount a standard, OCT system to enable concomitant data acquisition with both modalities while avoiding beam obscuration. The system was fed with a bottle beam comprised of a $p = 0$, $\ell = 4$ Laguerre-Gaussian mode with a 12.5-mm beam waist radius for increased throughput. The 50-mm focal length system was determined with ray tracing and simulated with an in-house physical optics code using a PEC sphere as a test target. The power coupling coefficient between the feed beam and scattered beam varied from 0.35 at 220 GHz to 0.48 at 330 GHz. While the system demonstrated a clear phase center at less than 1 λ from the geometric focal point, significant edge diffraction prevents the formation of a spherical phasefront, which is needed to achieve phase front matching.**

***Index Terms*— cornea sensing, Schwarzschild objective, submillimeter waves.**

I. Introduction

The aim of this work is to explore the design of a double reflector, quasi-optical system to implement cornea sensing at submillimeter frequencies. Submillimeter waves are a promising technology to realize water content measurements in biological tissues as the water permittivity is very high as well as dispersive at their frequencies, especially in WR3.4 frequency band. In particular, submillimeter waves can be used to realize in-vivo sensing of outer tissues such as cornea [1, 2] or skin [3] as penetration depth of the waves is limited by significant water absorption. We previously proposed refractive designs [4, 5] to realize cornea reflectometry but they have the disadvantage of being challenging to align without an additional sensor. As a next step, we would like to integrate the submillimeter wave system to operate along with an optical coherence tomography system (OCT), which is an established technology to image the anterior chamber of the eye. In this integrated system, the OCT can be used to image the cornea as well as to help to ascertain the alignment of the eye with the double reflector objective. If the target is aligned, or possibly, if the position of the target is well known with a certain precision, it should be possible to solve the inverse scattering problem and extract the target permittivity at submillimeter waves. At these frequencies, the cornea permittivity is expected to be a strong function of its water content. For the two channels, submillimeter-wave and OCT objectives, to be operating at the same time, they need to capture the scattered radiation from the cornea without blocking each other beam paths: An idea would be to perform peripheral corneal sensing, where the submillimeter wave illuminates the cornea within a ring. It could be therefore possible to exploit the double reflector blockage to locate the OCT as illustrated in Fig. 1. A suitable design for the double reflector could be a Schwarzschild objective as its spherical reflectors are easy to fabricate and it can be made aplanatic across a broad frequency range. Furthermore, the goal is to obtain a spherical wavefront that can match the corneal surface curvature. In ray tracing, this condition can be verified by looking at the rays'optical path length, whereas in Physical Optics (PO) one can look at the electric field phase distribution.

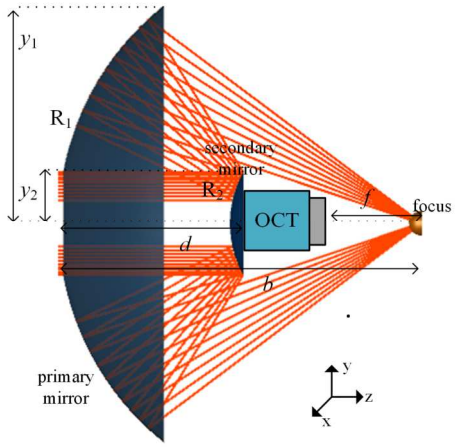

Fig. 1 Schwarzschild design CAD. The system comprises two spherical mirrors that guide a bottle of collimated rays and focus them at a point with distance *b* (2) from the feeding aperture. In this figure, the rays are drawn only on the y-z plane from the feed to the focus. The OCT system is located behind the secondary mirror.

II. Schwarzschild Objective Design

The Schwarzschild objective is a double reflector design which comprises a primary and secondary spherical mirrors [6].The two mirrors are concentric. A CAD of the system is shown in Fig. 1. The aplanatic design has two degrees of freedom: The focal length f and the aperture semidiameter of the feed y_2. The model was based on the following equations:

$$d = 2f \quad (1)$$

$$b = (\sqrt{5} + 2)f \quad (2)$$

$$R_1 = (\sqrt{5} + 1)f \quad (3)$$

$$R_2 = (\sqrt{5} - 1)f \quad (4)$$

$$y_1 = (\sqrt{5} + 2)y_2 \quad (5)$$

where d is the distance between the two mirrors, b is the geometrical optics focal length (GOF), R_1 is the radius of curvature the primary mirror, R_2 is the radius of curvature of the secondary mirror, and y_1 is the aperture semidiameter of the primary mirror. Previously explored optical designs utilized 60-mm clear aperture thus y_2 was fixed at 30 mm. The focal length f was set to 50 mm. The values of y_2 and f create a volume behind the secondary mirror approximately large enough to accommodate the presence of an optical coherence tomography (OCT) scanning objective.

III. Ray Tracing

Sequential ray tracing was performed via Zemax OpticStudio. The Schwarzschild system was fed with a hollow collimated bottle of rays; similar to those used in optical microscope objective design [6]. The ray paths went firstly through the secondary (R2) and primary (R1) mirrors, were reflected by a third spherical mirror of radius 7.5 mm (representing cornea), and the paths were also traced back till the feed aperture. Cornea has a typical radius of curvature value of 7.87 mm [7]. The optical path-length difference (OPD) feature of Zemax OpticStudio was used to compute the optical path from surface to surface. The setup uses a collimated bottle of rays, in an afocal system thus justifying OPD at the feed aperture, expressed in wavelength fractions as an appropriate metric. Additionally, a well-behaved wavefront is a requirement for a successful coupling at the transceiver. The ray tracing simulation was performed at 275 GHz and the ray field was polarized along the x-axis. The reflected ray paths are shown in Fig. 2 (a), and they closely resemble the forward paths in Fig. 1. The OPD error map is shown in Fig.Fig. 2 (b). The root mean square error (RMS) is small; ~0.0076 wavelengths. As expected, the wavefront error is low when the cornea sphere center of curvature is located concomitant with the focus as defined in (2). The wavefront error is below 0.07 wavelengths, which indicates that the system is diffraction limited. The wavefront error is small considering the relatively large wavelength, which is about 1 mm.

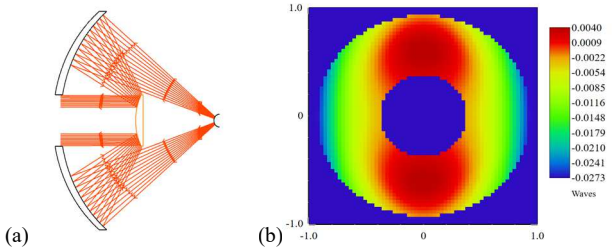

Fig. 2 (a) Reflected ray-tracing path. (b) OPD error expressed in wavelength fractions on the feed surface. The effect of the polarization is clearly visible as the error differs on the two different orthogonal axes.

IV. Physical Optics

The design was also evaluated with in-house PO code to verify the ray-tracing results. The PO algorithm runs sequentially from surface to surface, by computing the electric field propagated on each reflector. The system was fed with a bottle beam to match the ray tracing design. A candidate field is the Laguerre-Gaussian mode of radial mode $p = 0$ and azimuthal mode $\ell = 4$, for a beam waist radius ω_0 of 12.5 mm. The electric field at the feeding was modeled as:

$$E_{p,\ell}(r,0) = E_0\sqrt{\frac{2p!}{\pi(p+|\ell|)!}}\,\mathrm{L}_{p,\ell}^{|\ell|}\left(\frac{2r^2}{\omega_0^2}\right)\left(\frac{r\sqrt{2}}{\omega_0}\right)^{|\ell|}\exp\left(-\frac{r^2}{\omega^2(z)}\right) \qquad (6)$$

where $L_{p,\ell}$ is the generalized Laguerre polynomial and r is the radial coordinate. At these quasi-optical wavelengths, Laguerre-Gaussian beams are realizable with horn antennas [8], holograms, and metasurfaces [9] or approximated by a combination of axicon lenses. The simulations were done for the whole band from 220 GHz to 330 GHz with a step of 10 GHz and with a sampling rate of λ/2 or λ/6 depending on the surface.

A. PO field at the focus

The amplitude and phase of the co-polar component of the electric field at 270 GHz are shown in Fig. 3. The focus based on the ray tracing and the maximum point of the electric field amplitude of the co-polar component differ by less than λ at 270 GHz. Similarly, the maximum amplitude of the electric field coincides with the phase center. The phase center location is approximately constant across the WR3.4 frequency band as it varies by less than the minimum sampling step. The Arago spot, created by the secondary mirror blockage, is visible in both the amplitude and phase plots and it significantly perturbs the phase along the optical axis (x=0, Fig. 3 (b)). The wavefront deviates from the desired spherical profile and resembles the composition of three planar wavefronts. Side lobes in the amplitude are also most likely due to the blockage caused by the secondary mirror [10].

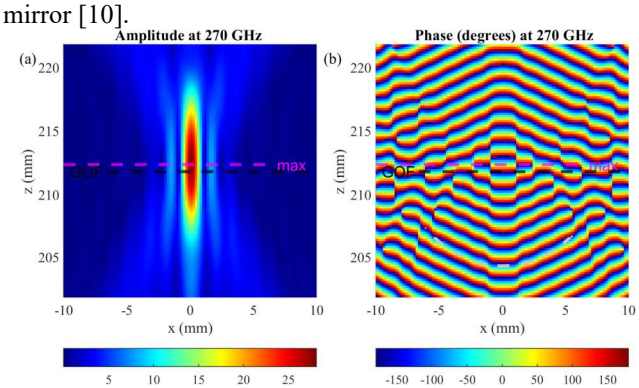

Fig.3 (a) The linear magnitude plot of the co-polar component of the electric field at 270 GHz. The electric field has a maximum at a less than a wavelength apart from the geometrical focus; (b) the phase contour plot of the co-polar component of electric field at 270 GHz. The magenta line corresponds to the maximum of the amplitude which also looks like to be the phase center (max). The black line corresponds to the geometrical optics focus (GOF) computed with (2). The gray dashed line represents the cornea surface.

B. Coupling with a spherical surface

A PEC spherical cap was placed so that its center of curvature was located at the geometrical optics focus to match the phase front radius analogously as done in Section III with ray tracing. The spherical cap had a radius of curvature of 7.5 mm

and an aperture diameter of 10.5 mm. In the previous section, the ray tracing results suggested that the wavefront error would be constrained at the final transceiver plane. The coupling between the scattered field from the sphere and the field incoming from the aperture feed was computed on the secondary mirror surface. The complex coupling coefficient was computed with the following formula:

$$\mathrm{K} = \frac{\iint_{S_2} E_{x,i} E_{x,r} \delta S_2}{\iint_{S_2} |E_{x,i}|^2 \delta S_2} \tag{7}$$

where $E_{\mathrm{x,i}}$ is the co-polar component of the incident electric field from the feed, $E_{\mathrm{x,r}}$ is the co-polar component of the electric field propagated from the secondary mirror and coming from the reflection path, and S_2 is the surface area of the secondary mirror. The magnitude of the complex coupling coefficient is represented in Fig. 4 (a) as a function of frequency. The coupling was computed both when the spherical cap's center of curvature was located at the geometrical optics focus and at the phase center. The result suggests that the coupling is potentially poor back at the transceiver for both locations, though it is slightly better with the phase center alignment. This may be because the wavefront is only approximately spherical. In Fig. 4 (b) and (c) the magnitude of the $E_{\mathrm{x,i}}$ and $E_{\mathrm{x,r}}$ at 270 GHz are also plotted. Their distributions indicate that poor coupling may be due to diffraction and energy loss arising from the secondary mirror obscuration. The effect of polarization is also visible, as the electric field amplitude is higher close to the *x*-axis, analogously to the ray-tracing plot Fig. 2(b).

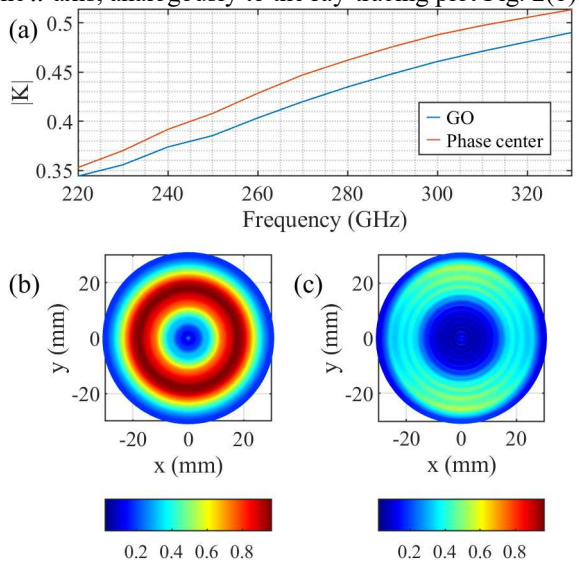

Fig. 4 (a) Coupling coefficient at the intermediate plane for the spherical cap center of curvature located at GOF. (b) Amplitude of $E_{\mathrm{x,i}}$ and (b) $E_{\mathrm{x,r}}$ at 270 GHz

V. Conclusion

A Schwarzschild objective was investigated for realizing sensing of spherical targets. Our physical-optics results indicate that the ray-tracing results are over-optimistic due to the diffraction-originated Arago spot and that the phase front is not as spherical as expected. The coupling coefficient is reduced by the out-of-phase wavefronts from the spherical mirrors and direct propagation into the Arago spot. Nevertheless, the coupling coefficient is good enough and this design offers the possibility to place the OCT objective on the optical axis. Broadband operation with this quasioptical design needs to be considered further. As next steps, we need to consider reducing the effects of diffraction, especially the Arago spot, by either mounting serrated or blended rolled edges or creating apodization on the mirrors. Ultimately, the design needs to be evaluated experimentally to verify its actual performance. A more accurate model for diffraction can also be used to evaluate the design such as unified theory of diffraction.

Acknowledgment

The calculations presented above were performed using computer resources within the Aalto University School of Science "Science-IT". This work is funded by Academy of Finland RADDESS programme (project AGRUM, decision number 327640).

References

[1] I. Ozheredov *et al.*, "In vivo THz sensing of the cornea of the eye," *Laser Physics Letters,* vol. 15, p. 055601, 2018.

[2] S. Sung *et al.*, "THz imaging system for in vivo human cornea," (in eng), *IEEE Trans Terahertz Sci Technol,* vol. 8, no. 1, pp. 27-37, 2018.

[3] A. Nikitkina *et al.*, "Terahertz radiation and the skin: a review," *Journal of Biomedical Optics,* vol. 26, no. 4, p. 043005, 2021.

[4] A. Tamminen, S. V. Pälli, J. Ala-Laurinaho, M. Salkola, A. V. Räisänen, and Z. D. Taylor, "Quasioptical System for Corneal Sensing at 220–330 GHz: Design, Evaluation, and Ex Vivo Cornea Parameter Extraction," *IEEE Trans Terahertz Sci Technol,* vol. 11, no. 2, pp. 135-149, 2021.

[5] A. Tamminen, S. Pälli, J. Ala-Laurinaho, M. Salkola, A. V. Räisänen, and Z. Taylor, "Axicon-hyperbolic lens for reflectivity measurements of curved surfaces," in *2020 14th European Conference on Antennas and Propagation (EuCAP)*, 2020, pp. 1-5.

[6] I. Artioukov and K. Krymski, "Schwarzschild objective for soft x-rays," *Optical Engineering,* vol. 39, no. 8, 2000.

[7] M. Dubbelman, H. A. Weeber, R. G. L. Van Der Heijde, and H. J. Völker-Dieben, "Radius and asphericity of the posterior corneal surface determined by corrected Scheimpflug photography," *Acta Ophthalmologica Scandinavica,* vol. 80, no. 4, pp. 379-383, 2002.

[8] C. D. R. Bocio, R. Gonzalo, M. S. Ayza, and M. Thumm, "Optimal horn antenna design to excite high-order Gaussian beam modes from TE/sub 0m/ smooth circular waveguide modes," *IEEE Transactions on Antennas and Propagation,* vol. 47, no. 9, pp. 1440-1448, 1999.

[9] W. Fu, S. Hu, C. Zhang, X. Guan, and Y. Yan, "Compact quasi-optical mode converter based on anisotropic metasurfaces," *Opt. Express,* vol. 29, no. 11, pp. 16205-16213, 2021.

[10] P. F. Goldsmith, *Quasioptical systems : Gaussian beam quasioptical propagation and applications* Piscataway, NJ: IEEE Press, 1998.